Optical fibre thermometry using ratiometric green emission of an upconverting nanoparticle-polydimethylsiloxane composite

Rahul Kumar[1]*, Leonardo Binetti[2], T. Hien Nguyen[1], Lourdes S M Alwis[2], Tong Sun[1], and Kenneth T V Grattan[1]

[1]Department of Electrical and Electronic Engineering, City, University of London, London, EC1V 0HB, United Kingdom

[2]School of Engineering and the Built Environment, Edinburgh Napier University, Edinburgh, EH10 5DT, United Kingdom

*Rahul.Kumar@city.ac.uk

ABSTRACT

The thermally coupled green band emission from excited Er^{3+} ions has been used in the past to create optical thermometers, by doping the material in various types of media, particularly glasses. Glasses are known to be excellent hosts for Er^{3+} ions: however, high temperatures (>900 K) are usually required for doping these ions into glasses and a non-linear temperature response is often produced. In this work, the frequently encountered drawbacks of glass-based temperature sensors have been addressed by developing a temperature sensor created at a lower temperature (543 K), by dip-coating chemically synthesized upconverting nanoparticles (UCNP – $NaYF_4$:(18%) Yb^{3+}, (2%) Er^{3+}) embedded in polydimethylsiloxane (PDMS) onto the tip of a 1000 μm optical fibre, to create the actual fibre probe. The sensor shows an excellent linear response ($R^2 = 0.991$) over a very useful temperature range of 295 K – 473 K, with a sensitivity of 2.9 $\times 10^{-3}$ K^{-1}, a temperature resolution of ± 2.7 K and response time of ~ 5 seconds. Additionally, a probe was investigated

where a pure upconverting nanoparticle powder was coated on the tip of optical fibre and its spectral and temperature response was obtained (and cross compared with that of UCNP-PDMS composite). The results obtained from the probe development work show that the UCNP-PDMS-coated optical fibre temperature sensor developed offers a better alternative to more conventional Er^{3+} doped glass-based temperature sensors, in terms of the thermal budget, the synthesis process and the ease of coating, creating as a result, a very linear device response.

KEYWORDS: Upconverting Nanoparticle, Polydimethylsiloxane, Optical temperature sensor, Optical Fibre, Organic-inorganic hybrid

1. Introduction

The importance of temperature measurement to industry can be judged from the fact that approximately 75-80% of the sensors available on the market are temperature sensors [1]. Among the available range of temperature sensors, optical fibre, fluorescence-based temperature detection is distinctive over conventional electrically-based detection for a number of reasons, including safety and immunity to stray electromagnetic radiation, for example [2,3]. Optical fibre-based temperature sensing devices using fluorescence from a well-chosen, appropriate material respond well to the demand for reliable and low-cost sensors needed for rugged environments, such as monitoring of transformers in a transmission grid and temperature monitoring in oil refineries, coal mines, electrical transport infrastructure and fire detection, where conventional measurement techniques may not be safe or subject to interference [4,5]. Optical fibre grating-based sensors can measure elevated temperatures, but often use expensive interrogation systems [6], whereas in comparison, fluorescence based detection can provide a lower-cost alternative solution due to relatively inexpensive excitation and detection techniques of the optical signals involved [7].

The most commonly used down-converting fluorescent materials, (i.e. those where $\lambda_{excitation} < \lambda_{emission}$) for temperature sensing are organic dyes and quantum dots [8,9]. However, organic dyes frequently suffer from a photo-bleaching effect, especially in the vapor phase and therefore cannot be used for extended periods [10]. Further, most quantum dot-based devices have problems with cytotoxicity and often use an excitation wavelength in the ultraviolet part of the spectrum, where prolonged exposure may cause photodecomposition of the samples [11]. These problems

associated with down-converting materials can be overcome by using another class of fluorescent materials know as up-converting (UC) materials where, as the term "upconversion" suggests, the emission of the shorter wavelength results from absorption of two or more longer wavelength (and therefore less energetic) photons. By comparison with conventional nonlinear UC techniques such as simultaneous two-photon absorption and second-harmonic generation, UC is achieved by sequential absorption of two or more such photons. Rare-earth (RE) group elements (mainly Er^{3+}, Ho^{3+} and Tm^{3+}) are a natural choice for low pump-intensity UC because of their ladder-like metastable energy bands, naturally created in the $4f^{n}$ electronic configuration due to electronic repulsion and spin-orbit coupling [12–14]. Furthermore, such RE^{3+} ions based on UC typically exhibit large anti-Stokes shifts [14], sharp emission lines [15] and temperature-dependent emissions, provided the two radiative energy levels have an energy difference of between 200 cm^{-1} and 2000 cm^{-1} [16–18]. The populations of these thermally coupled levels (TCL), related through the Boltzmann distribution, provide a natural ratiometric temperature detection approach, in that way reducing the influence of external conditions on the sensor performance and creating an inbuilt 'reference' channel [19–22].

As can be seen from the literature, Er^{3+} (or the combination of Er^{3+} and Yb^{3+}) has been widely used as a dopant in various types of glasses, such as tellurite [23–25], fluorotellurite [26], oxyfluoride [27,28], fluoroindate [29,30], chalcogenide [31] and fluorophosphate [32] glasses, serving as the basis of various fluorescence-based temperature sensors. A detailed review of various upconversion-based temperature sensor schemes has been produced by Zhao *et al*. in recently published review paper [33] . Since the doping of RE^{3+} ions in glass is generally performed in the molten phase, a high temperature environment for the synthesis is needed (with temperatures usually rising to more than 900 K). Furthermore, the experimental arrangements needed for the operation of several of the sensors reported are relatively complex (requiring lenses, collimators, a bulky spectrometer etc.) and thus are expensive and susceptible to environmental effects [23,26,28,31,32], making them less well suited to be used outside the laboratory. To avoid the problems that are experienced when a high temperature environment is used during synthesis, in this work an upconverting nanoparticle (UCNP)-polydimethylsiloxane (PDMS) composite has been explored as the basis of the sensor system itself – one that is created at much lower temperatures (583 K) than glasses.

The characterization of these potential sensor materials (prior to their incorporation in the sensor probe itself) is done using where a sample of this UCNP-PDMS composite was dip coated on a multimode, larger diameter, optical fibre (chosen to allow the maximum excitation light to be delivered to the sensor head and light collected from it), with an inexpensive portable USB-based spectrometer was used to record fluorescence. The use of optical fibre also provides the advantage of high signal-to-noise ratio, potentially long distances being possible between the point where the sensing is occurring (particularly valuable in applications such as mining) and offering reliability of performance in corrosive & harsh environments [34]. Since, it was not possible to dope RE^{3+} ions directly into the PDMS, a hexagonal-phased UCNP (NaYF$_4$: (18%) Yb^{3+}; (2%) Er^{3+}) composite was used as the basis of the sensor material. This approach was preferred over the use of other UC nanoparticle materials because of their high UC efficiency [35]. Similarly, PDMS was chosen over other polymers because of its good chemical stability, resistance to water, low cost and good optical properties in the visible-near infra-red (NIR) region (such as high transparency and low autofluorescence [36]). Moreover, PDMS shows good adhesion to glass, which further simplifies the coating process onto optical fibres and thus increases the lifetime of the sensor created.

In this paper, UCNP has been chemically synthesized using a solvothermal method and its fluorescence emission has been explored and recorded, in three different media i.e. in a non-polar solvent (cyclohexane), in powder and in PDMS. Following that, the UC powder itself and the UCNP-PDMS composite materials created have been coated onto multi-mode optical fibre, to form the basis of the temperature sensors designed, ready for evaluation. The optical fibre thermometer schemes thus developed has been characterized and a 'figure of merit' for the sensors obtained. This has been designed to make a cross-comparison of key parameters more easy: the figure of merit has been determined from the data captured on the temperature-related change in the ratios of the integrated emission intensities of the two green emission bands, from the Er^{3+} ions.

2. Experimental Section

A. *Chemicals and Reagents*

For the chemical synthesis of the UCNP, the following chemicals were used: Yttrium(III) chloride hexahydrate (YCl$_3\cdot$6H$_2$O; 99.99%; Acros Organics), Ytterbium(III) chloride hexahydrate

(YbCl$_3$·6H$_2$O; 99.90%; Acros Organics), Erbium(III) chloride hexahydrate (ErCl$_3$·6H$_2$O; 99.90%; Sigma Aldrich), Ammonium fluoride (NH$_4$F; ≥98.0%; Acros Organics), Sodium Hydroxide (NaOH, 97+%; Sigma Aldrich), Methanol (Analytical Grade, Fisher Scientific), Ethanol (HPLC grade; Fisher Scientific), Oleic acid (C$_{18}$H$_{34}$O$_2$; 90%; Sigma Aldrich), 1-Octadecene (C$_{18}$H$_{36}$; 90%; Sigma Aldrich), Cyclohexane (C$_6$H$_{12}$; > 95%; Acros Organics), and silver conductive paint (Electrolube). PDMS (SYLGARD 184) was purchased from Dowsil. All chemicals were used as received without any further purification.

B. *Thermometer Materials Characterization – Instrumentation used*

The transmission electron microscope (TEM) imaging was done using a Model JEM-1010, operating at an accelerating voltage of 80kV. The hydrodynamic diameter of the UCNP was calculated using a Zetasizer Nano ZEN 3600 (Malvern Instruments). The attenuated total reflection Fourier-Transform InfraRed (ATR-FTIR) spectra were obtained using a Perkin Elmer Frontier Spectrometer.

C. *Synthesis of UCNP & UCNP-PDMS Composites*

The hexagonal phase UNCP used in this work was chemically synthesized using a solvothermal process, by slightly modifying the procedure described elsewhere [37]. In summary, 0.8 mmol of YCl$_3$·6H$_2$O, 0.18 mmol of YbCl$_3$·6H$_2$O and 0.02 mmol of ErCl$_3$·6H$_2$O, 15 ml of 1-octadecane (acting as solvent) and 6 ml of oleic acid (acting as surfactant) were added to a 50 ml three-necked round-bottom glass flask. Heating was applied to the above mixture, taking it to a temperature of 433 K for 30 mins in an inert (argon) environment to dissolve the lanthanide salts while stirring at 350 rpm (throughout the synthesis process the solution was kept stirred at this speed). After cooling the solution to room temperature i.e. ~297 K, 2.5 mmol of NaOH and 3.9 mmol of NH$_4$F dissolved in 3 ml and 10 ml methanol solution respectively were added dropwise, using a 20 ml syringe. This is a crucial step because NaOH and NH$_4$F rapidly react to form a NaF precipitate which tends to stick to the walls of the beaker and the amount of NaF added to the solution determines the size and shape uniformity of the UCNP thus created [38]. Therefore, to avoid the NaF sticking to the walls of the beaker, instead of mixing the NaOH and NH$_4$F methanol-based solutions in a beaker and then transferring the NaF precipitate to the syringe, these methanol-

based solutions were mixed directly in the syringe itself for convenience. Afterwards, the resultant solution was kept stirred at 323 K for 30 minutes to complete the NaF nucleation process. In the next step, the methanol was completely removed from the solution by gradually heating it to 383 K (alternating between argon flow and vacuum pressure during the ramping process) and once the temperature reached 383 K, it was maintained there for 10 minutes under vacuum conditions. Thereafter, the solution was quickly ramped up to 583 K (at a rate of 10 K/min) and kept at that temperature for one hour under argon protection, before cooling down naturally. Once the solution was cooled down, it was transferred to a 50 ml centrifuge tube, mixed thoroughly with 5 ml of ethanol and the resultant solution was centrifuged at 3500g for 3 minutes. After discarding the supernatant, the white-colored precipitant was re-dispersed into cyclohexane and again precipitated by adding 8 ml of ethanol, following which centrifugation (3500g for 3 minutes) was carried out. The previous step was repeated once more by replacing 8 ml of ethanol by 4 ml of ethanol and 4 ml of methanol. Finally, the precipitant was re-dispersed in 4 ml of fresh cyclohexane to obtain a stable, transparent UCNP colloidal solution (concentration: 0.05 mg/µl), as shown in Fig. 1(a).

UCNP-PDMS was obtained by modifying the steps used by Wang *et al.* [39]. As a first step, UCNP colloidal solution, PDMS base solution and the curing agent were placed (in a ratio 10:10:1 (by volume)) in a glass beaker and mixed thoroughly. The bubble trapped in the resultant solution, while mixing, was removed by degassing it in a vacuum chamber for half an hour. Afterwards, the solution was left overnight, at room temperate and pressure. The following morning, the partially cured solution was heated to 354 K (below the cyclohexane flash point) for an hour to ensure the complete removal of the cyclohexane, while at the same time completing the curing process.

D. Optical Fibre Thermometer Design

A 5 cm long polymer clad silica multimode Optical Fibre (OF), having 1000 µm core diameter (FT1000UMT; Thorlabs) was used as the basis of the temperature probe itself. An OF with a 1000 µm core diameter was chosen because this larger diameter (than used for typical 'communications-grade' fibre) not only provides a much large surface area for coating, excitation and recollection of the UC fluorescence but also offers good mechanical strength to the probe. To increase the light coupling efficiency, both end facets were sequentially polished flat using 5 µm, 3 µm and 1 µm grit polishing sheet (LFG series, Thorlabs). Finally, 1 cm of polymer jacket was removed from

one end of the fibre, which was glued to a SMA connector (11050A; Thorlabs) while from another end 1.5 cm of polymer jacket and 5 mm of cladding were removed. The bare facet was used for coating with the UC powder and UCNP-PDMS to create the probes.

For the UC powder coating, first UCNP was precipitated from a 500 µl of colloidal solution by adding 500 µl of ethanol followed by centrifugation (3500 g, 3 mins). After discarding the supernatant, the bare end of the OF was inserted into the precipitate to attach some UC powder to the fibre tip. Finally, the UC powder-coated OF was dried overnight and heated at 354 K for an hour (the following morning) to remove any residual traces of cyclohexane.

To coat the UCNP-PDMS composite, the 3 mm of optical fibre was dipped in the UCNP-PDMS composite solution, obtained by mixing UCNP and PDMS and removing the trapped bubbles that were seen and which would deteriorate the optical quality of the probe material (as described above). It was then left for one minute and slowly taken out using a lab-jack. As in the case of the UC powder, the UCNP-PDMS was left overnight at room temperature and pressure and the next morning heated to 354 K for an hour. Another 5 mm layer of PDMS was coated on the fibre, following the same procedure but with the exception of replacing the UCNP-PDMS solution by PDMS. This PDMS coating passivates the Er^{3+} ions present on the surface of UCNP-PDMS, thus nullifying the impact of the surrounding environment on the UC fluorescence. Since the OF probe was designed to operate in reflection-mode, silver paint was coated on the tip by dipping it into commercially-obtained silver paint, thus to enhance the reflection of UC fluorescence. The probe created in this way is shown in Fig. 1(b). In that figure, the inset shows the visible (green) UC fluorescence emitted by the UCNP-PDMS-coated tip, upon excitation using light from a 500 mW, 980 nm wavelength (λ) laser source. Before evaluating the temperature sensing performance of the probe, it was annealed at 503 K for 3 hours to stabilize it.
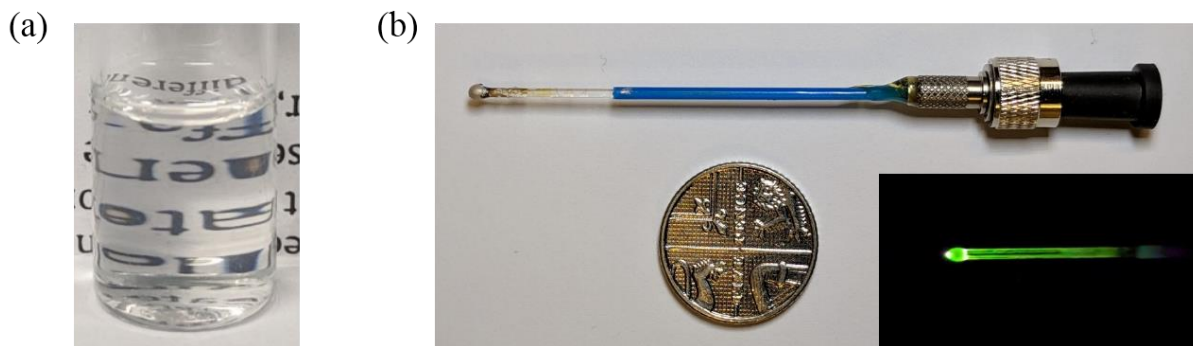
(a)   (b)

Figure 1 Photograph of (a) UCNP dispersed in cyclohexane (illustrating the clarity of the solution) (b) Optical fibre temperature probe constructed after coating silver paint on the UCNP-PDMS tip. Inset shows green UC fluorescence emitted by UCNP-PDMS coated tip (before the silver coating was applied) upon excitation with light from a 500 mW, 980 nm laser source.

E. Optical Thermometer Characterization Setup

In all the experiments carried out to investigate the fluorescence-based performance of the sensor probe, light from a continuous-wave 980 nm diode laser (JDSU 2900 series) with a fibre pigtail and a maximum achievable power (of 500 mW) was used for excitation. The UC fluorescence emitted was acquired using a portable spectrometer (Maya-type 2000PRO; Ocean Optics), while the UC spectrum of the colloidal solution was recorded using the setup created (and shown in online supplementary Fig. S1). The laser source and the spectrometer were connected to 1 cm cuvette holder (CUV-ALL-UV; Ocean Optics), set at 90° to each other to minimize the amount of scattered source light reaching the spectrometer.

The UC powder and the UCNP-PDMS were coated onto the OF, following the steps described in the preceding subsection and characterized using the setup shown in Fig. 2. As can be seen from the setup shown in Fig. 2(a), the laser source and the spectrometer were connected to the two ends of 2x1 fibre bundle (ϕ = 230 μm; Ocean Optics), while the third was connected to the coated OF probe through an SMA connector (SMA905, L-com). A 2 mm thick NIR rejection filter (ϕ = 11.9 mm; BP550; MidOpt) was placed in the path of the spectrometer to avoid its saturation from the reflected source light. The NIR filter was mounted on a 1 cm cuvette holder (CUV-UV; Ocean Optics; shown in online supplementary Fig. S2) as it provides a natural alignment between the

incoming and the outgoing fibre, thus making the setup both simple and readily portable when required. The UC spectrum was recorded over the wavelength range from 400 nm to 700 nm (at a resolution of 1 nm), with an integration time of 1 second, using the Spectra Suit software package (Ocean Optics).

In the experiments which were set up to investigate the temperature performance of the probe, a heater (RCT Basic; IKA) equipped with a thermocouple (ETS-DS; IKA; minimum resolution = 0.1 K) was used to regulate and control the temperate of a sand bath (SiO_2; 50-70 mesh particle size; Sigma Aldrich) or air bath, to provide a stable temperature zone for the calibration. The sand bath, due to its excellent thermal properties, was used to decrease the ramping-up time, minimize the temperature fluctuations and achieve a uniform temperature distribution, which facilitated the calibration of the probe. For each temperature, the mean value of six replicated readings, taken at intervals of 1 minute, was recorded.
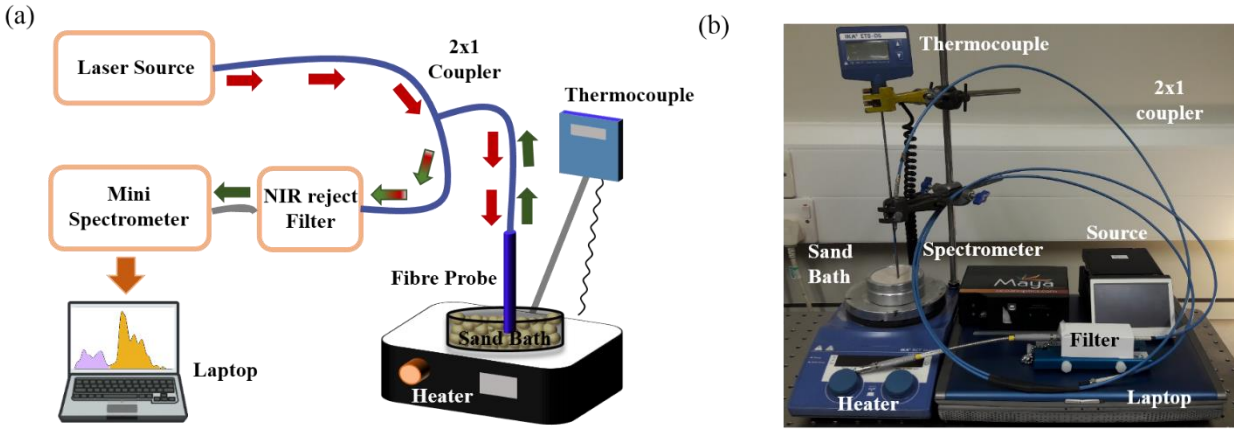

Figure 2: Thermal characterization of the probes (a) Schematic of the setup used showing the key components (b) Photograph of the equipment used in the experimental calibration

3. Results and discussion

A. *Characterization of the Thermometer materials*

A TEM image of the synthesized UCNP used is shown in the Fig. 3(a). It can be seen from the figure that the synthesized UCNPs are of uniform size and have a clear hexagonal shape, as desired.

The mean hydrodynamic diameter of the UCNPs was found to be ~56 nm from the DLS measurement made. The inset of Fig. 3(a) shows the green visible UC fluorescence emitted by the synthesized colloidal solutions on excitation with light from a 500 mW, 980 nm diode laser. Figure 3(b) shows photographs of the PDMS (marked as 1) and the UCNP-PDMS composite (marked as 2) and the UCNP-PDMS when excited with light from a 980 nm diode laser (marked as 3). It can be seen from the same figure that the UCNP-PDMS composite is less transparent than the pristine PDMS. This loss of transparency on adding the UCNP to the PDMS results from the agglomeration of the UCNP to form strong scattering centers, as observed and reported in the literature for other inorganic-organic nanocomposites [40,41]. The loss of transparency does not have significant impact on its usage as a temperature sensing material.
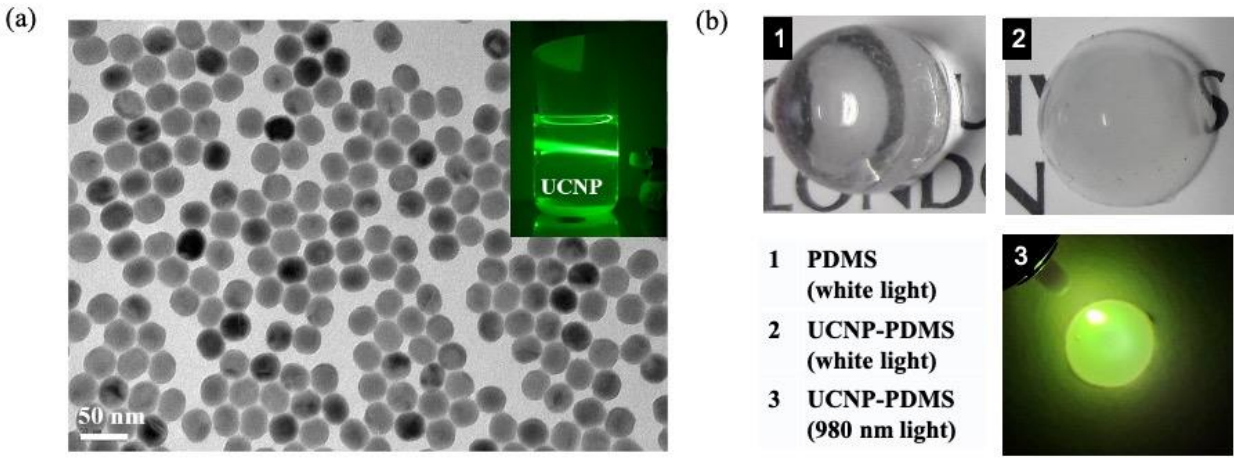

Figure 3 (a) TEM image of synthesized hexagonal phased-UCNP. Inset shows the green UC fluorescence from the UCNP colloidal solution when excited using light from the 980 nm laser source. (b) Photographs of the PDMS (marked as 1) and the UCNP-PDMS composite (marked as 2) and UCNP-PDMS when excited with light from the 980 nm diode laser (marked as 3).

Figure 4 shows the UC emission spectra recorded using the spectrometer mentioned, for UCNPs in three different media: in cyclohexane, as powder and in PDMS. It can be seen that in all the three media the UC fluorescence shows three distinctive peaks (marked as 1, 2 and 3 on the figure) and these comprise two 'green' bands (λ_{peak} = 525 nm & 545 nm) and one 'red' band (λ_{peak} = 650 nm). The electronic transitions responsible for these peaks are shown in relation to the energy level diagram given in Fig. 4(b). As previously described in the literature [12–14], the energy level $^4I_{11/2}$ is populated through several routes but the energy transfer (ET) from Yb^{3+} ($^2F_{5/2}$ (Yb^{3+})

10

+ $^4I_{15/2}$ (Er^{3+}) → $^2F_{7/2}$ (Yb^{3+}) + $^4I_{11/2}$ (Er^{3+})) and through ground state absorption (GSA; $^4I_{15/2}$ (Er^{3+}) + photon → $^4I_{11/2}$ (Er^{3+})) are dominant. Further, contrasting the ET and the GSA mentioned above, the probability of the occurrence of ET is greater than GSA, due to the higher absorption coefficient of the Yb^{3+} ions (when compared to that for Er^{3+} ions) at the input wavelength used [13,25]. For the green band emission, electrons excited from $^4I_{11/2}$ to $^4F_{7/2}$ through ET ($^2F_{5/2}$ (Yb^{3+}) + $^4I_{11/2}$ (Er^{3+}) → $^2F_{7/2}$ (Yb^{3+}) + $^4F_{7/2}$ (Er^{3+})) or excited state absorption (ESA; $^4I_{11/2}$ (Er^{3+}) + photon → $^4F_{7/2}$ (Er^{3+})), quickly settle into more stable states $^2H_{11/2}$, $^4S_{3/2}$, through non-radiative phononic relaxation. The emission bands around 523 nm and 545 nm arise due to the radiative transition of electrons from $^2H_{11/2}$ → $^4I_{15/2}$ and $^4S_{3/2}$ → $^4I_{15/2}$ respectively. For the red band transition ($^4F_{9/2}$ → $^4I_{15/2}$), the energy level $^4F_{9/2}$ is populated via two major routes. The first of these is through the de-excitation of electrons from $^4I_{11/2}$ to $^4I_{13/2}$ through phononic relaxation and then excitation from $^4I_{13/2}$ to $^4F_{9/2}$ through ET ($^2F_{5/2}$ (Yb^{3+}) + $^4I_{13/2}$ (Er^{3+}) → $^2F_{7/2}$ (Yb^{3+}) + $^4F_{9/2}$ (Er^{3+})) or ESA ($^4I_{13/2}$ (Er^{3+}) + photon → $^4F_{9/2}$ (Er^{3+})). In the second route, $^4F_{9/2}$ becomes populated through non-radiative relaxation from $^4S_{3/2}$.
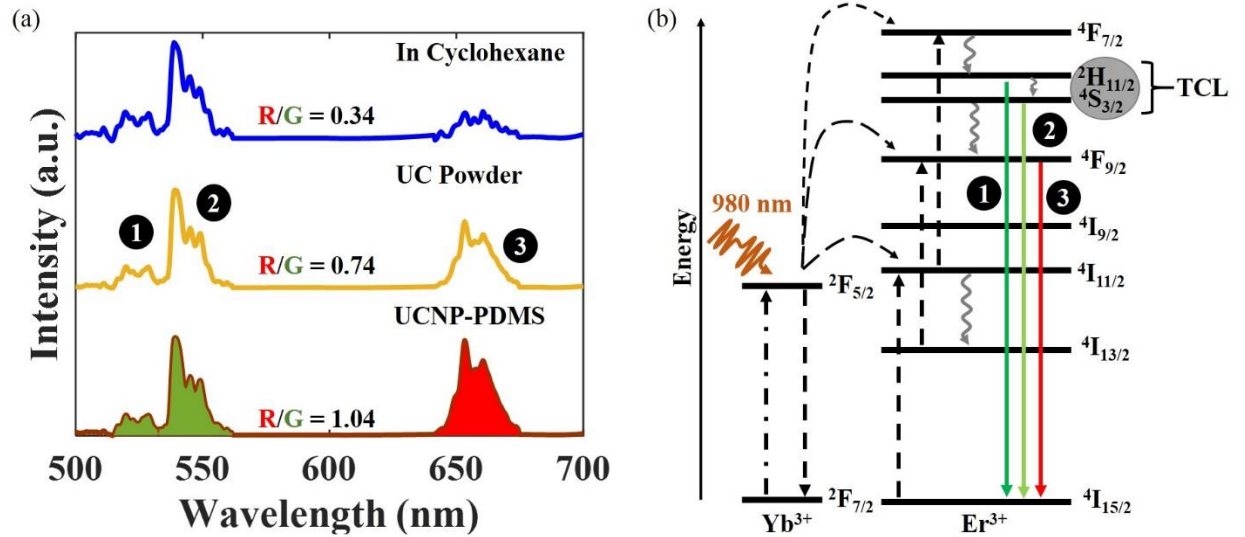

Figure 4 UC emission spectra when UCNP is dispersed in cyclohexane, UC powder & UCNP-PDMS. R/G represents the integrated intensities of the red and green bands, shown by red and green colored areas in the lower spectrum shown (b) Partial energy level diagram of Yb^{3+}/Er^{3+} showing the important radiative and non-radiative transitions involved in the UC mechanism. The

dash-dotted, dashed, wavy and solid line represent the NIR photon excitation, energy transfer, multi-phonon relaxation and emission processes respectively.

As discussed in the previous paragraph and evident from the energy level diagram shown in Fig. 4(b), the intensities of the red and green emissions are related through the non-radiative transition between $^4I_{11/2} \rightarrow ^4I_{13/2}$ and $^4S_{3/2} \rightarrow ^4F_{9/2}$, which in turn are strongly affected by the surface properties of the particles, such as surface defects, proximate impurities, surface states, attached ligands, etc. [42]. Therefore, it can be seen from Fig. 4(a) that the Red to Green ratio (R/G) is different for all three media. The increase in the R/G ratio in the powder form, in comparison to the colloidal solution UCNP, has been observed previously and has been attributed to an increase in the cross-relaxation energy transfer between the Er^{3+}- Er^{3+} surface ions, due to the clustering of the Er^{3+} ions in the powder [43]. In the case of the UCNP-PDMS composite, the observed R/G was highest among the three media considered. This could be due to combined effect of cross-relaxation between the Er^{3+} - Er^{3+} ions at agglomerated sites and an increase in the non-radiative relaxation between the $^4S_{3/2}$ and $^4F_{9/2}$ levels, caused by the presence of the CH_3 lateral chain of the PDMS near the surface. As can be seen from the ATR-FTIR of the UCNP-PDMS composite, shown in Fig. 5(a), the vibrational energy of the C-H stretching (2962 cm^{-1}) is closer to the energy gap of $^4S_{3/2} \rightarrow ^4F_{9/2}$ (3200 cm^{-1}), thus increasing the probability of multiphoton relaxation on the transition $^4S_{3/2} \rightarrow ^4F_{9/2}$.
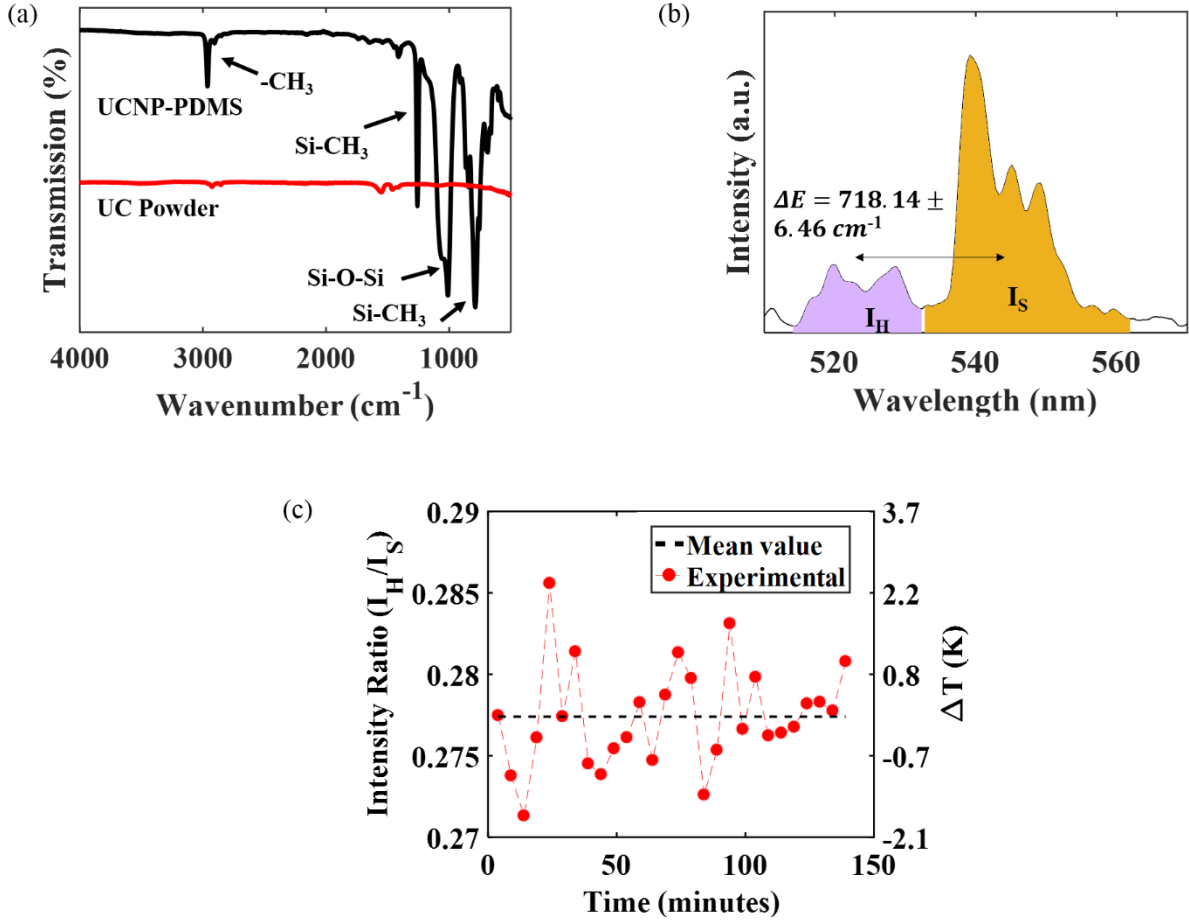
Figure 5 (a) ATR-FTIR response of UC powder and UCNP-PDMS composite (b) Green UC emission bands of Er^{3+} ions. I_H is the area under curve from 514 nm to 532.3 nm corresponding to the radiative transition $^2H_{11/2} \rightarrow {}^4I_{15/2}$ and I_S is the area under curve from 532.8 nm to 562 nm corresponding to the radiative transition $^4S_{3/2} \rightarrow {}^4I_{15/2}$ (c) Variation of Intensity ratio (I_H/I_S) with time due to laser source heating. The right axis shows the variation of temperature with respect to the mean value.

B. *Temperature response of UC Powder-based thermometer*

As mentioned above, the ratio of the integrated emission intensities of the green bands under quasi-thermal equilibrium follows Boltzmann's distribution, in accordance with Eq. 1.

$$R = \frac{I_H}{I_S} = \frac{g_H \omega_H A_H}{g_S \omega_S A_S} e^{\left(\frac{-\Delta E}{k_B T}\right)} = B e^{\left(\frac{-\Delta E}{k_B T}\right)},$$

(1)

13

where I_H is the area under the emission intensity curve between the 514 nm and 532.3 nm peaks, as shown by the purple area in Fig. 5(b) and I_S is the area under the emission intensity curve over the wavelength range 532.8 nm to 562 nm (shown by yellow area in Fig. 5(b)). g, ω, and A are the degeneracy of the given energy level, the angular frequency of the radiative transitions from the same energy level to the ground level and the emission cross-section respectively, $\varDelta E$ is the energy gap between the $^2H_{11/2}$ and $^4S_{3/2}$ levels, k_B is Boltzmann's constant and T is the temperature. The pre-exponential constant B is given by $(g_H\omega_H A_H/g_S\omega_S A_S)$. The area under the curve was calculated using Simpson's rule and ΔE was obtained by calculating the difference between the barycenter of I_H and I_S and the corresponding standard error, δE, is the error in difference across temperature. The barycenter of the corresponding emission was calculated using Eq. 2 and the value obtained of $\Delta E = 718.14 \pm 6.46$ cm^{-1} is in good agreement with the previously reported values [28,44] .

$$\overline{E} = 10^7 * \left(\frac{\sum_{\lambda_1}^{\lambda_2} \lambda I(\lambda)}{\sum_{\lambda_1}^{\lambda_2} I(\lambda)} \right)^{-1} \tag{2}$$

Before calibrating the response of the sensor to the external change in temperature, any self-heating due to the laser source that may be present was monitored, over a period of 2.5 hours. Fig. 5(c) shows the fluctuation of the intensity ratio (IR) over that period (left axis) and the corresponding temperature fluctuation on the right axis (the mean value of the fluctuation of the IR is considered as a reference). It can be seen from the figure that the temperature variation is within the temperature resolution of the sensor (± 2.7 K: calculation shown later). Moreover, the IR of the sensor remained the same even on reducing the laser source power by half, i.e. 250 mW. These results prove that it is a reasonable assumption that any heating due to the laser source is unimportant.

The variation in the intensity of the green fluorescence of the UC powder, recorded with an increase in temperature from 298 K to 398 K, is shown in Fig. 6(a). It can be seen from the main figure and the inset that I_H increases and I_S decreases with the increase in temperature. The ratio of I_H and I_S as function of temperature, as shown in Fig. 6(b), fits excellently ($R^2 = 0.999$) with the function shown in Eq. 1, thus indicating that the increase in I_H and the corresponding decrease in I_S are due to the thermal transfer of electrons from energy level $^4S_{3/2}$ to $^2H_{11/2}$. The value of $\Delta E =$

777.15 cm^{-1}, obtained from the fitting, is in good agreement with the value obtained from a barycenter calculation (718.14 ± 6.46 cm^{-1}). The value obtained for the pre-exponential factor *B* also matches well with previously reported values in literature [23,45,46]. Since, the Eq. 1 does not take into account the temperature-dependent non-radiative transition rates from $^4S_{3/2}$ and $^2H_{11/2}$, the close fitting of the experimental data to Eq. 1 shows that the phonon-assisted non-radiative recombination rate is insignificant over the given temperature range, for the UC powder. Moreover, the intensity ratio variation, with temperature can also be approximated to a linear function over the given temperature range, with R^2 = 0.996, as shown in Fig. 7(a).
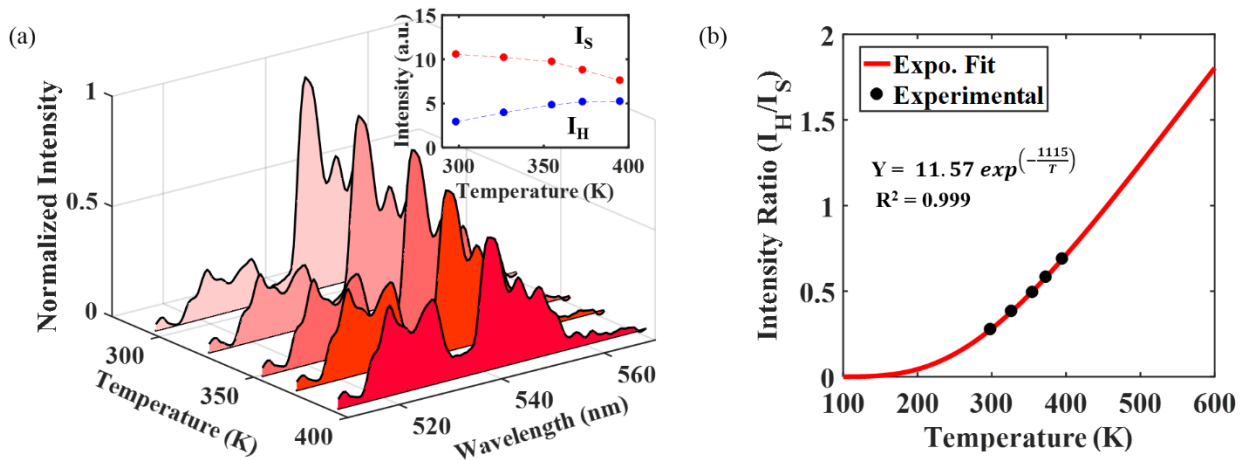

Figure 6 UC powder: (a) Variation of green fluorescence with temperature. The figure has been normalized to the maximum value (obtained at 297 K). The inset shows variation of I_H and I_S with temperature. (b) Experimentally obtained ratio of I_H and I_S against temperature, juxtaposed with an exponential fitting using Eq. 1.

The absolute thermal sensitivity (S_A) and the relative thermal sensitivity (S_R) of the thermometer are given by Eq. 3 and Eq. 4 respectively. It can be seen from Fig. 7(b) that S increases with temperature and the maximum value obtained for S was (4.913 ± 0.018) ×10^{-3} K^{-1} at 394.9 ± 0.5 K, whereas S_R monotonically decreases from (12.535 ± 0.031)×10^{-3} K^{-1} to (7.148 ± 0.023)×10^{-3} K^{-1} with the increase in temperature from 298.2 ± 0.1 K to 394.9 ± 0.5 K. The minimum resolution of the temperature (δT) that could be determined using Eq. 5 and Eq. 6, was ± 2.7 K. In Eq. 6, δI_H and δI_S are the standard errors (standard deviation divided with the square root of the number of repeated measurements made, i.e. 6 in the present case) in I_H and I_S respectively.

$$S_A = \frac{dR}{dT} = R\left(\frac{\Delta E}{k_B T^2}\right) \tag{3}$$

$$S_R = \frac{1}{R}\frac{dR}{dT} = \left(\frac{\Delta E}{k_B T^2}\right) \tag{4}$$

$$\delta T = \frac{\delta R}{S} \quad ,where \tag{5}$$

$$\delta R = R\sqrt{\left(\frac{\delta I_H}{I_H}\right)^2 + \left(\frac{\delta I_S}{I_S}\right)^2} \tag{6}$$
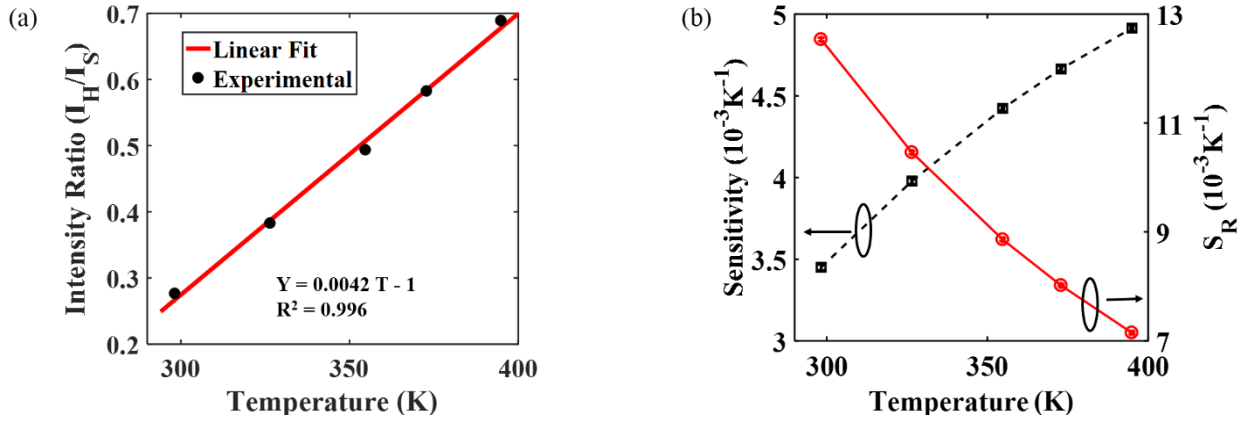

Figure 7 (a) Linear fitting of the ratio obtained of I_H and I_S over the temperature range from 298 K to 395 K (b) Absolute (left) and relative (right) thermal sensitivities obtained for the UC powder.

Since, the adhesion of the UC powder to the optical fibre was not strong in comparison to UCNP-PDMS composite, the probe lifetime reduces considerably as the coating is lost from the fibre, with time, in normal use.

C. Temperature response of UCNP-PDMS Composite based thermometer

The variation in the green fluorescence bands of the UCNP-PDMS composite-coated probe is shown in Fig. 8(a). It can be seen from the main figure and the inset (showing the integrated intensity) that that rate of decrease of I_S with temperature is more than for the UC Powder, whereas in contrast to I_S, the rate of increase in I_H is smaller. Furthermore, the variation of the ratio of I_H/I_S with temperature, as shown in Fig. 8(b), shows an excellent linear fit ($R^2 = 0.991$), but unlike the UC powder, this does not fit as well ($R^2 = 0.89$) with Eq. 1, as shown in Fig. 9(a). In the above

fitting, $\Delta E = 727.65$ cm^{-1} (calculated from Eq. 2) was used. The low R-squared value illustrates that thermal transfer of electrons from $^4S_{3/2} \rightarrow {}^2H_{11/2}$ is not strictly governed by the Boltzmann distribution. The deviation of the thermal response of the UCNP-PDMS composite from the Boltzmann distribution can be attributed to the increase in the temperature-dependent non-radiative transitions [47] due to presence of the PDMS chemical bonds, as revealed from the ATR-FTIR spectrum (ref. Fig. 5(a)), in the vicinity of the surface of Er^{3+} ions.
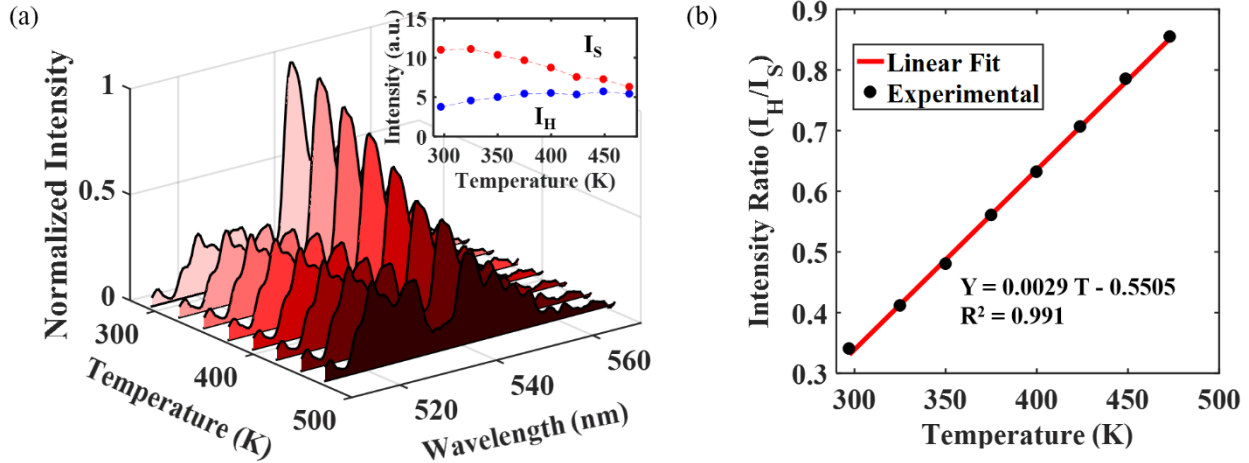

Figure 8: UCNP-PDMS composite coated probe: (a) Variation in green fluorescence bands with temperature. The inset shows integrated emission intensities (b) Linear fitting of the experimentally obtained ratio of (I_H/I_S), as function of temperature

The performance of the sensor created using this material shows a linear temperature response and the same sensitivity of $(2.9 \pm 0.4) \times 10^{-3}$ K^{-1} across its working temperature range, a positive feature not usually shown by earlier Er^{3+}, Er^{3+}/Yb^{3+} doped glass-based temperature sensors. The reduction in the thermal sensitivity of the UCNP-PDMS composite (with respect to the UC powder $(4.913 \pm 0.018) \times 10^{-3}$ K^{-1}) is again due to the reduction in the energy transfer efficiency, owing to the high non-radiative losses. The same pattern was observed in the case of glass-based temperature sensors where glasses having high phonon energies (such silicate and oxide-based glasses) show a lower sensitivity in comparison to glasses having a low phonon energy, such as tellurite glass [25]. The cyclical response of the sensor and the smoothened curve obtained by calculating the mean from 20 neighboring points is shown by both solid and dotted lines respectively, by varying the temperature from 296 K to 359 K (and back) is shown in Fig. 9(b). From these data, the response

time of the sensor, (defined as the time seen on the rising curve between a 10% and 90% peak level i.e. (t_{90}-t_{10})) was found to be ~ 5 seconds. The temperature resolution ± 2.7 K, calculated using Eq. 5 & Eq. 6, was the same as that for the UC powder. Also, although the silver coating on the tip of sensor is not essential, it increases the overall UC green fluorescence intensity by ~ 23% (as shown in online supplementary Fig. S3). Further work on increasing the observed fluorescence intensity received is underway and the use of different, thinner coatings may help here. However, it is noted that the use of a silver coating does enhance the performance.
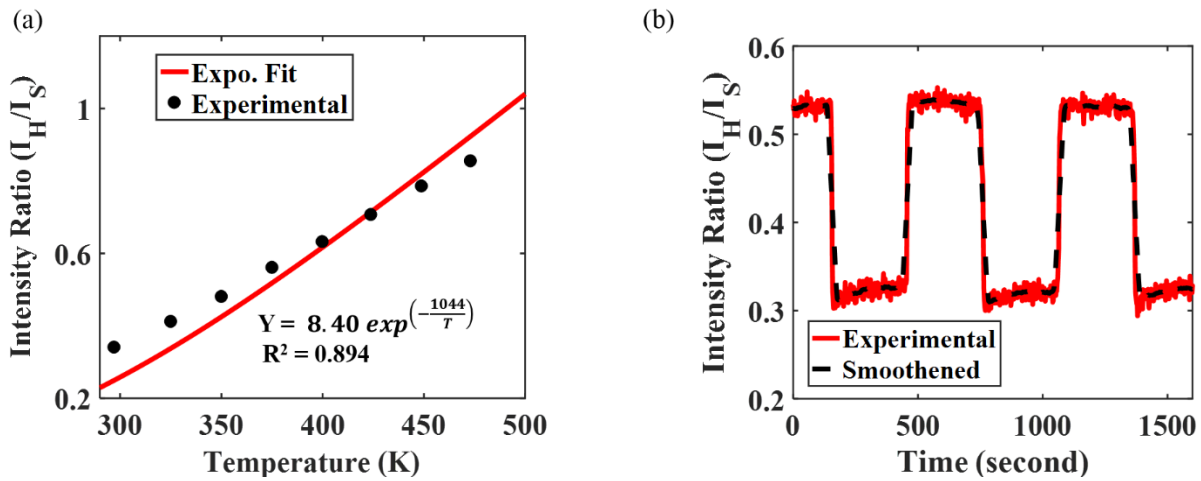

Figure 9: (a) Exponential fitting of the experimentally obtained ratio of (I_H/I_S) as function of temperature, using Eq. 1 (b) Cyclic response obtained through repeatedly varying the temperature from 296 K to 359 K (and back). The smoothened curve (dotted) was obtained by calculating local mean from 20 neighboring points is shown as guidance for the eyes.

The UCNP-PDMS composite probe shows a repeatable temperature response, measured over a period of several months, benefitting from the good adhesion between the PDMS and the optical fibre (OF) used.

D. *Comparison of performance with previous sensors*

In order to compare the performance of the probes developed and in this work evaluated, their thermal responses were compared to those of a number of others using published information from

the literature, collating published data on Er^{3+} or Er^{3+}/Yb^{3+} doped glass-based temperature sensor devices. The minimum sensitivity value of the sensors reported has been extracted from the sensitivity curve of the work of Rohatgi et al [48], using the webplot digitizer tool . As can be seen from Table 1, the UCNP-PDMS-based temperature sensor developed shows a maximum sensitivity of 2.9×10^{-3} K^{-1}, but where this device has the advantage of having been fabricated at lower temperatures. Further, unlike most of the sensors previously reported, the maximum sensitivity of this device remains constant across the full operating temperature range, emphasizing the value for applications where such a strongly linear response is desirable.

Table 1: Comparison of key parameters of the performance of probes developed in this work with those from Er^{3+}/Yb^{3+} doped glass temperature sensors, reported in the literature

Doped material as the basis of the sensor	Maximum synthesis temperature needed (K)	S_{max} (Temp) 10^{-3} K^{-1} (K)	S_{min} (Temp) 10^{-3} K^{-1} (K)	Sensor Operational temperature Range (K)	Response	Literature Reference
UCNP-PDMS composite	**583**	**2.9 (295)**	**2.9 (295)**	**295-473**	**Linear**	**This work**
UC Powder	**583**	**4.9 (395)**	**3.5 (295)**	**295-395**	**Exponential/ Linear**	**This work**
Er^{3+}/Yb^{3+}: tellurite glass	973	8.9 (473)	2.1 (278)	278-473	Piecewise Linear	[25]
Er^{3+}/Yb^{3+}: TeO$_2$–WO$_3$ glass	1023	2.8 (690)	2.1 (300)	300–690	Exponential	[23]
Er^{3+}/Yb^{3+}: fluorotellurite glasses	1073	5.4 (568)	3.6 (298)	298-568	Exponential	[49]
Er^{3+}/Yb^{3+}: germinate tellurite glass	1173	3.6 (493)	2.1 (293)	293-493	Linear	[24]
Er3+: Bi$_3$Ti$_{1.5}$W$_{0.5}$O$_9$ ceramic	1373	3.1 (423)	1.8 (83)	83-423	Exponential	[50]
Er^{3+}: PbO-Ga$_2$O$_3$-SiO$_2$ glass	1373	2.6 (592)	0.5 (298)	298–650	Exponential	[45]
Er^{3+}: oxyfluoride glass	1473	2.7 (450)	1.8 (250)	250–450	Exponential	[28]
Er^{3+}/Yb^{3+}: silicate glass	1723	3.3 (296)	1.8 (723)	296–723	Exponential	[51]
Er^{3+}: KYb$_2$F$_7$ nanocrystal in fluoride glass ceramics	1823	14 (300)	5.4 (480)	300–480	Exponential	[52]

Er^{3+}/Yb^{3+}: K_3LuF_6 nanocrystal in oxyflouride glass ceramic	1823	14 (300)	2.1 (773)	300-773	Exponential	[53]
Er^{3+}: Sr_2YbF_7 glass ceramics	1823	6.1 (500)	3.8(300)	300-500	Exponential	[54]
Er^{3+}/Yb^{3+}: β-$NaGdF_4$ nanocrystals glass ceramic	1863	3.7 (563)	2.3 (303)	303-563	Exponential	[55]

4. Conclusion

In the work carried out using ratiometric green emission of an upconverting nanoparticle-polydimethylsiloxane composite, practical and simple designs for optical fibre-based thermometers using both UC powder and UCNP-PDMS composites have been developed and their performance reported. The sensor materials have been synthesized and coated on a multimode optical fibre, to create useable sensor platforms and the best of these was selected and explored further. Even though the UC powder showed a higher thermal sensitivity than the UCNP-PDMS composite ($S_{UC\ powder}$ = (4.913 ± 0.018)×10^{-3} K^{-1}; $S_{UCNP-PDMS}$ = (2.9 ± 0.4)×10^{-3} K^{-1}), the latter is preferable for many applications over the former due to the stable coating arising from the good adhesion between the PDMS and the optical fibre. The optimum UCNP-PDMS coated thermometer thus created shows an excellent linear temperature response over the important range 298 K to 493 K, with a same order of sensitivity as had previously been reported for several Er^{3+}/Yb^{3+} doped glass-based sensors, but achieved more simply through a room temperature coating technique. The work has emphasized the advantages of the low temperature synthesis process: the ease of the coating technique, the simple and portable characterization setup used and the creation and optimization of a physically robust probe, all demonstrating the value of this low temperature approach to create a practical and inexpensive sensor system, which can be undertaken in a typical chemical synthesis laboratory. Future work will explore several other UCNP-polymer composites for a variety of additional sensing applications, taking advantage of this low temperature synthesis approach.

Author Contributions

R.K. did synthesis, probe preparation, thermal characterization and wrote the manuscript. T.H.N. assisted in synthesis of nanoparticles. L.B & L.A. performed DLS & ATR-FTIR measurement. T.S. and K.G. supervised the research.

Competing Interests

Authors declare no competing interests.

REFERENCES

[1]   Market Research Report, Temperature Sensors Market Analysis By Application (Automotive, Consumer Electronics, Environmental, Medical, Process Industries) and Segment Forecasts to 2020, San Francisco, 2015. https://doi.org/ISBN 978-1-68038-495-6.

[2]   K.T.V. Grattan, P. A.W, Wilson, A miniaturised microcomputer-based neodymium "decay-time" temperature sensor, J. Phys. E. 20 (1987) 1201–1205. https://doi.org/10.1088/0022-3735/20/10/010.

[3]   K.T.V. Grattan, A.W. Palmer, Infrared fluorescence "decay-time" temperature sensor, Rev. Sci. Instrum. 56 (1985) 1784–1787. https://doi.org/10.1063/1.1138094.

[4]   X.D. Wang, O.S. Wolfbeis, R.J. Meier, Luminescent probes and sensors for temperature, Chem. Soc. Rev. 42 (2013) 7834–7869. https://doi.org/10.1039/c3cs60102a.

[5]   C.D.S. Brites, S. Balabhadra, L.D. Carlos, Lanthanide-Based Thermometers: At the Cutting-Edge of Luminescence Thermometry, Adv. Opt. Mater. 7 (2019) 1801239.

https://doi.org/10.1002/adom.201801239.

[6]   S. Pal, J. Mandal, T. Sun, K.T.V. Grattan, M. Fokine, F. Carlsson, P.Y. Fonjallaz, S.A. Wade, S.F. Collins, Characteristics of potential fibre Bragg grating sensor-based devices at elevated temperatures, Meas. Sci. Technol. 14 (2003) 1131–1136. https://doi.org/10.1088/0957-0233/14/7/331.

[7]   Z.Y. Zhang, K.T.V. Grattan, A.W. Palmer, B.T. Meggitt, T. Sun, Fluorescence decay-time characteristics of erbium-doped optical fiber at elevated temperatures, Rev. Sci. Instrum. 68 (1997) 2764–2766. https://doi.org/10.1063/1.1148192.

[8]   L.M. Maestro, C. Jacinto, U.R. Silva, F. Vetrone, J.A. Capobianco, D. Jaque, J.G. Solé, CdTe quantum dots as nanothermometers: Towards highly sensitive thermal imaging, Small. 7 (2011) 1774–1778. https://doi.org/10.1002/smll.201002377.

[9]   H.F. Arata, P. Löw, K. Ishizuka, C. Bergaud, B. Kim, H. Noji, H. Fujita, Temperature distribution measurement on microfabricated thermodevice for single biomolecular observation using fluorescent dye, Sensors Actuators, B Chem. 117 (2006) 339–345. https://doi.org/10.1016/j.snb.2005.11.017.

[10]   R.H. Compton, K.T.V. Grattan, T. Morrow, Photophysical parameters for potential vapour-phase dye-laser media, Appl. Phys. 22 (1980) 307–311. https://doi.org/10.1007/BF00899883.

[11]   Y. Wang, W. Cao, S. Li, W. Wen, Facile and high spatial resolution ratio-metric luminescence thermal mapping in microfluidics by near infrared excited upconversion nanoparticles, Appl. Phys. Lett. 108 (2016). https://doi.org/10.1063/1.4940746.

[12]   F. Auzel, Upconversion and Anti-Stokes Processes with f and d Ions in Solids, Chem. Rev. 104 (2004) 139–173. https://doi.org/10.1021/cr020357g.

[13]   M. Haase, H. Schäfer, Upconverting nanoparticles, Angew. Chemie - Int. Ed. 50 (2011) 5808–5829. https://doi.org/10.1002/anie.201005159.

[14]   B. Zhou, B. Shi, D. Jin, X. Liu, Controlling upconversion nanocrystals for emerging applications, Nat. Nanotechnol. 10 (2015) 924–936.

https://doi.org/10.1038/nnano.2015.251.

[15]   K. Binnemans, Lanthanide-based luminescent hybrid materials, Chem. Rev. 109 (2009) 4283–4374. https://doi.org/10.1021/cr8003983.

[16]   S. Zheng, W. Chen, D. Tan, J. Zhou, Q. Guo, W. Jiang, C. Xu, X. Liu, J. Qiu, Lanthanide-doped NaGdF4 core-shell nanoparticles for non-contact self-referencing temperature sensors, Nanoscale. 6 (2014) 5675–5679. https://doi.org/10.1039/c4nr00432a.

[17]   S.F. León-Luis, U.R. Rodríguez-Mendoza, P. Haro-González, I.R. Martín, V. Lavín, Role of the host matrix on the thermal sensitivity of Er 3+ luminescence in optical temperature sensors, Sensors Actuators, B Chem. 174 (2012) 176–186. https://doi.org/10.1016/j.snb.2012.08.019.

[18]   B. Dong, T. Yang, M.K. Lei, Optical high temperature sensor based on green up-conversion emissions in Er3+ doped Al2O3, Sensors Actuators, B Chem. 123 (2007) 667–670. https://doi.org/10.1016/j.snb.2006.10.002.

[19]   S. Balabhadra, M.L. Debasu, C.D.S. Brites, R.A.S. Ferreira, L.D. Carlos, Upconverting Nanoparticles Working As Primary Thermometers in Different Media, J. Phys. Chem. C. (2017). https://doi.org/10.1021/acs.jpcc.7b04827.

[20]   H. Suo, C. Guo, J. Zheng, B. Zhou, C. Ma, X. Zhao, T. Li, P. Guo, E.M. Goldys, Sensitivity Modulation of Upconverting Thermometry through Engineering Phonon Energy of a Matrix, ACS Appl. Mater. Interfaces. (2016). https://doi.org/10.1021/acsami.6b12176.

[21]   V.K. Rai, Temperature sensors and optical sensors, Appl. Phys. B Lasers Opt. 88 (2007) 297–303. https://doi.org/10.1007/s00340-007-2717-4.

[22]   A. Li, D. Xu, H. Lin, S. Yang, Y. Shao, Y. Zhang, NaGd(MoO4)2 nanocrystals with diverse morphologies: Controlled synthesis, growth mechanism, photoluminescence and thermometric properties, Sci. Rep. 6 (2016). https://doi.org/10.1038/srep31366.

[23]   A. Pandey, S. Som, V. Kumar, V. Kumar, K. Kumar, V.K. Rai, H.C. Swart, Enhanced upconversion and temperature sensing study of Er3+-Yb3+ codoped tungsten-tellurite glass, Sensors Actuators, B Chem. 202 (2014) 1305–1312.

https://doi.org/10.1016/j.snb.2014.06.074.

[24] M. Kochanowicz, D. Dorosz, J. Zmojda, J. Dorosz, P. Miluski, Influence of temperature on upconversion luminescence in tellurite glass co-doped with Yb3+/Er3+ and Yb3+/Tm 3+, J. Lumin. 151 (2014) 155–160. https://doi.org/10.1016/j.jlumin.2014.02.012.

[25] D. Manzani, J.F. da S. Petruci, K. Nigoghossian, A.A. Cardoso, S.J.L. Ribeiro, A portable luminescent thermometer based on green up-conversion emission of Er3+/Yb3+ co-doped tellurite glass, Sci. Rep. 7 (2017) 41596. https://doi.org/10.1038/srep41596.

[26] S.F. León-Luis, U.R. Rodríguez-Mendoza, I.R. Martín, E. Lalla, V. Lavín, Effects of Er3+ concentration on thermal sensitivity in optical temperature fluorotellurite glass sensors, Sensors Actuators, B Chem. 176 (2013) 1167–1175. https://doi.org/10.1016/j.snb.2012.09.067.

[27] W. Xu, H. Zhao, Z. Zhang, W. Cao, Highly sensitive optical thermometry through thermally enhanced near infrared emissions from Nd3+/Yb3+ codoped oxyfluoride glass ceramic, Sensors Actuators, B Chem. 178 (2013) 520–524. https://doi.org/10.1016/j.snb.2012.12.050.

[28] L. Feng, B. Lai, J. Wang, G. Du, Q. Su, Spectroscopic properties of Er3+ in a oxyfluoride glass and upconversion and temperature sensor behaviour of Er3+/Yb3+-codoped oxyfluoride glass, J. Lumin. 130 (2010) 2418–2423. https://doi.org/10.1016/j.jlumin.2010.08.005.

[29] P. Haro-González, S.F. León-Luis, S. González-Pérez, I.R. Martín, Analysis of Er3+ and Ho3+ codoped fluoroindate glasses as wide range temperature sensor, Mater. Res. Bull. 46 (2011) 1051–1054. https://doi.org/10.1016/j.materresbull.2011.03.010.

[30] G.S. et al. Maciel, Temperature sensor based on frequency upconversion in Er3+-doped fluoroindate glass, IEEE Photon. Technol. Lett. 7 (1995) 1474–1476.

[31] P. V Dos Santos, M.T. De Araujo, A.S. Gouveia-Neto, J.A.M. Neto, A.S.B. Sombra, Optical Thermometry Through Infrared Excited Upconversion Fluorescence Emission in Er3+- and Er3+-Yb3+-doped Chalcogenide Glasses, IEEE J. Quantum Electron. 35 (1999) 395.

https://doi.org/10.1109/3.748846.

[32] B. Lai, L. Feng, J. Wang, Q. Su, Optical transition and upconversion luminescence in Er3+ doped and Er3+-Yb3+ co-doped fluorophosphate glasses, Opt. Mater. (Amst). 32 (2010) 1154–1160. https://doi.org/10.1016/j.optmat.2010.03.023.

[33] Y. Zhao, X. Wang, Y. Zhang, Y. Li, X. Yao, Optical temperature sensing of up-conversion luminescent materials: Fundamentals and progress, J. Alloys Compd. 817 (2020). https://doi.org/10.1016/j.jallcom.2019.152691.

[34] J. Cao, M.H. Tu, T. Sun, K.T.V. Grattan, Wavelength-based localized surface plasmon resonance optical fiber biosensor, Sensors Actuators, B Chem. 181 (2013) 611–619. https://doi.org/10.1016/j.snb.2013.02.052.

[35] A. Aebischer, M. Hostettler, J. Hauser, K. Krämer, T. Weber, H.U. Güdel, H.B. Bürgi, Structural and spectroscopic characterization of active sites in a family of light-emitting sodium lanthanide tetrafluorides, Angew. Chemie - Int. Ed. 45 (2006) 2802–2806. https://doi.org/10.1002/anie.200503966.

[36] A. Piruska, I. Nikcevic, S.H. Lee, C. Ahn, W.R. Heineman, P.A. Limbach, C.J. Seliskar, The autofluorescence of plastic materials and chips measured under laser irradiation, Lab Chip. 5 (2005) 1348–1354. https://doi.org/10.1039/b508288a.

[37] L. Liang, A. Care, R. Zhang, Y. Lu, N.H. Packer, A. Sunna, Y. Qian, A. V. Zvyagin, Facile Assembly of Functional Upconversion Nanoparticles for Targeted Cancer Imaging and Photodynamic Therapy, ACS Appl. Mater. Interfaces. 8 (2016) 11945–11953. https://doi.org/10.1021/acsami.6b00713.

[38] F. Wang, R. Deng, X. Liu, Preparation of core-shell NaGdF4 nanoparticles doped with luminescent lanthanide ions to be used as upconversion-based probes, Nat. Protoc. 9 (2014) 1634. https://doi.org/10.1038/nprot.2014.111.

[39] F. Wang, Y. Han, C.S. Lim, Y. Lu, J. Wang, J. Xu, H. Chen, C. Zhang, M. Hong, X. Liu, Simultaneous phase and size control of upconversion nanocrystals through lanthanide doping, Nature. 463 (2010) 1061. https://doi.org/10.1038/nature08777.

[40] H. Althues, R. Palkovits, A. Rumplecker, P. Simon, W. Sigle, M. Bredol, U. Kynast, S. Kaskel, Synthesis and characterization of transparent luminescent ZnS:Mn/PMMA nanocomposites, Chem. Mater. 18 (2006) 1068–1072. https://doi.org/10.1021/cm0477422.

[41] S. Lee, H.J. Shin, S.M. Yoon, D.K. Yi, J.Y. Choi, U. Paik, Refractive index engineering of transparent ZrO2- polydimethylsiloxane nanocomposites, J. Mater. Chem. 18 (2008) 1751–1755. https://doi.org/10.1039/b715338d.

[42] N. Bogdan, F. Vetrone, G.A. Ozin, J.A. Capobianco, Synthesis of ligand-free colloidally stable water dispersible brightly luminescent lanthanide-doped upconverting nanoparticles, Nano Lett. 11 (2011) 835–840. https://doi.org/10.1021/nl1041929.

[43] H. Schäfer, P. Ptacek, R. Kömpe, M. Haase, Lanthanide-doped NaYF4 nanocrystals in aqueous solution displaying strong up-conversion emission, Chem. Mater. 19 (2007) 1396–1400. https://doi.org/10.1021/cm062385b.

[44] C.D.S. Brites, X. Xie, M.L. Debasu, Instantaneous ballistic velocity of suspended Brownian nanocrystals measured by upconversion nanothermometry, Nat. Nanotechnol. 11 (2016) 851. https://doi.org/10.1038/nnano.2016.111.

[45] W.A. Pisarski, J. Pisarska, R. Lisiecki, W. Ryba-Romanowski, Sensitive optical temperature sensor based on up-conversion luminescence spectra of Er3+ ions in PbO–Ga2O3–XO2 (X = Ge, Si) glasses, Opt. Mater. (Amst). 59 (2016) 87–90. https://doi.org/10.1016/j.optmat.2016.01.037.

[46] S.F. León-Luis, U.R. Rodríguez-Mendoza, E. Lalla, V. Lavín, Temperature sensor based on the Er3+ green upconverted emission in a fluorotellurite glass, Sensors Actuators, B Chem. 158 (2011) 208–213. https://doi.org/10.1016/j.snb.2011.06.005.

[47] L.A. Risebergt, H.W. Moos, Multiphonon Orbit-Lattice Relaxation of Excited States of Rare-Earth Ions in Crystals, Phys. Rev. 174 (1968) 429. https://doi.org/https://doi.org/10.1103/PhysRev.174.429.

[48] A. Rohatgi, Webplotdigitizer, Version 4.2. (2019). https://automeris.io/WebPlotDigitizer (accessed March 3, 2020).

[49]   X. Huang, J. Liu, H. Pan, C. Tian, H. Zhang, X. Chen, A. Huang, Z. Xiao, Temperature-dependent upconversion luminescence and spectra characteristic of Er 3+ /Yb 3+ co-doped fluorotellurite glasses, J. Lumin. 207 (2019) 41–47. https://doi.org/10.1016/j.jlumin.2018.10.028.

[50]   Y. Zhang, J. Li, X. Chai, X. Wang, Y. Li, X. Yao, Enhanced electrical properties, color-tunable up-conversion luminescence, and temperature sensing behaviour in Er-doped Bi3Ti1.5W0.5O9 multifunctional ferroelectric ceramics, J. Appl. Phys. 121 (2017) 0–7. https://doi.org/10.1063/1.4979096.

[51]   C. Li, B. Dong, S. Li, C. Song, Er3+-Yb3+ co-doped silicate glass for optical temperature sensor, Chem. Phys. Lett. 443 (2007) 426–429. https://doi.org/10.1016/j.cplett.2007.06.081.

[52]   J.K. Cao, F.F. Hu, L.P. Chen, H. Guo, C. Duan, M. Yin, Optical thermometry based on up-conversion luminescence behavior of Er3+-doped KYb2F7nano-crystals in bulk glass ceramics, J. Alloys Compd. 693 (2017) 326–331. https://doi.org/10.1016/j.jallcom.2016.09.163.

[53]   J.K. Cao, F.F. Hu, L.P. Chen, H. Guo, C. Duan, M. Yin, Wide-range thermometry based on green up-conversion luminescence of K3LuF6:Yb3+/Er3+ bulk oxyfluoride glass ceramics, J. Am. Ceram. Soc. 100 (2017) 2108–2115. https://doi.org/10.1111/jace.14606.

[54]   X. Li, J. Cao, Y. Wei, Z. Yang, H. Guo, Optical Thermometry Based on Up-Conversion Luminescence Behavior of Er3+ -Doped Transparent Sr2YbF7 Glass-Ceramics, J. Am. Ceram. Soc. 98 (2015) 3824–3830. https://doi.org/10.1111/jace.13804.

[55]   D. Chen, Z. Wan, Y. Zhou, P. Huang, J. Zhong, M. Ding, W. Xiang, X. Liang, Z. Ji, Bulk glass ceramics containing Yb3+/Er3+: β-NaGdF4 nanocrystals: Phase-separation-controlled crystallization, optical spectroscopy and upconverted temperature sensing behavior, J. Alloys Compd. 638 (2015) 21–28. https://doi.org/10.1016/j.jallcom.2015.02.170.

SUPPLEMENTARY INFORMATION

Optical fibre thermometry using ratiometric green emission of an upconverting nanoparticle-polydimethylsiloxane composite

Rahul Kumar[1]*, Leonardo Binetti[2], Hien T Nguyen[1], Lourdes S Alwis[2], Tong Sun[1], and Kenneth T V Grattan[1]

[1]Department of Electrical and Electronics Engineering, City, University of London, EC1V 0HB, United Kingdom

[2]School of Engineering and the Built Environment, Edinburgh Napier University, Edinburgh, EH10 5DT, United Kingdom

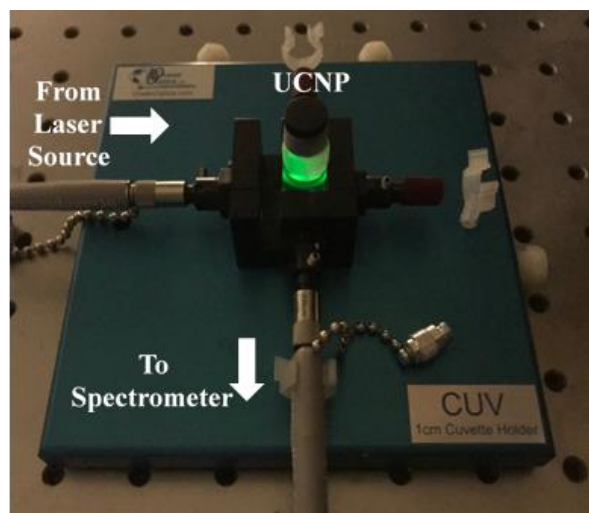Email: *Rahul.Kumar@city.ac.uk

Figure 4: Characterization setup for measuring fluorescence of UCNP in colloidal solution. During measurement, external light was turned off.
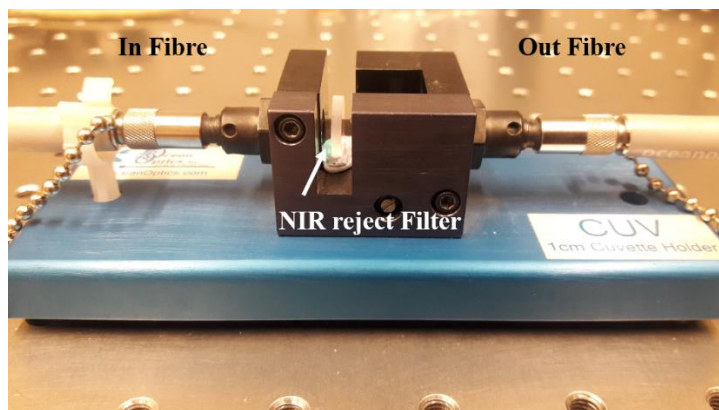

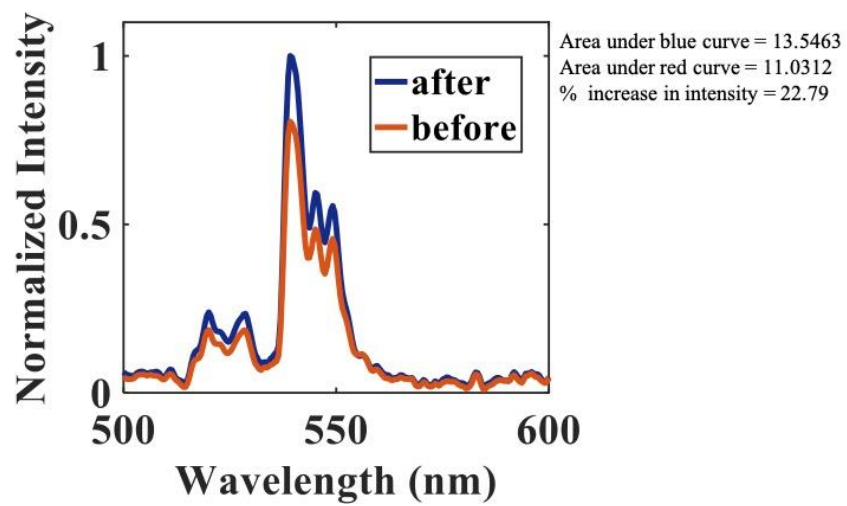Figure 5: NIR filter holder used in thermal characterization setup

Figure 3: Normalized Green Fluorescence before and after coating of commercial silver paint.